

# Temporal coherence effects in multiple ionization of N<sub>2</sub> via XUV pump-probe autocorrelation

Y. H. Jiang,<sup>1</sup> T. Pfeifer,<sup>1</sup> A. Rudenko,<sup>2</sup> O. Herrwerth,<sup>3</sup> L. Foucar,<sup>2</sup> M. Kurka,<sup>1</sup> K. U. Kühnel,<sup>1</sup> M. Lezius,<sup>3</sup> M. F. Kling,<sup>3</sup> X. Liu,<sup>4</sup> K. Ueda,<sup>4</sup> S. Düsterer,<sup>5</sup> R. Treusch,<sup>5</sup> C. D. Schröter,<sup>1</sup> R. Moshhammer,<sup>1</sup> and J. Ullrich<sup>1,2</sup>

<sup>1</sup>Max-Planck-Institut für Kernphysik, D-69117 Heidelberg, Germany

<sup>2</sup>Max-Planck Advanced Study Group at CFEL, D-22607 Hamburg, Germany

<sup>3</sup>Max-Planck-Institut für Quantenoptik, D-85748 Garching, Germany

<sup>4</sup>Institute of Multidisciplinary Research for Advanced Materials, Tohoku University, 980–8577 Sendai, Japan

<sup>5</sup>DESY, D-22607 Hamburg, Germany

(Received 4 August 2010; published 19 October 2010)

Using a split-mirror stage combined with a reaction microscope, nonlinear autocorrelation traces of XUV pulses from the Free-electron LASer at Hamburg were recorded for N<sub>2</sub> multiphoton-induced fragmentation into noncoincident N<sup>2+</sup> and coincident N<sup>2+</sup> + N<sup>2+</sup> channels. We find a pulse duration of  $40 \pm 10$  fs along with a sharp spike pointing to a coherence time of  $4 \pm 1$  fs, almost twice as short as in previous observations. Both are well reproduced by a simulation based on the partial-coherence model that includes the molecular dynamics leading to an  $\sim 12$ -fs substructure in the trace.

DOI: 10.1103/PhysRevA.82.041403

PACS number(s): 33.80.Eh, 41.60.Cr, 42.65.Re

Among the most outstanding recent breakthroughs in laser technology is the advent of fourth-generation light sources, the free-electron lasers (FELs), delivering XUV to hard x-ray pulses with unprecedented peak brilliance—nine orders of magnitude larger than in synchrotrons—and ultrashort pulse durations down to a few femtoseconds with attoseconds being in reach. Thus, we enter a new regime in x-ray-matter interactions with unforeseeable consequences in physics, chemistry, and potentially, in biology. Across the disciplines, one of the most fascinating common goals is to visualize, as a function of time, ultrafast structural changes in a very general sense, spanning from the electronic structure of correlated materials, atomic positions in (bio)molecules during chemical reactions to correlations in liquids or warm dense matter. Even though various attempts to seed the lasers are underway, all existing FELs, the SPring-8 Compact SASE (Self-Amplified Spontaneous Emission) Source test facility [1], FLASH (the Free-electron LASer at Hamburg) [2], and the Linac Coherent Light Source [3] are currently operated in the SASE mode. Here, lasing starts from the shot noise of individual electron bunches, thus, leading to significant shot-by-shot variations of the properties of single emitted FEL light pulses with respect to their intensity as well as of their temporal and spectral shapes. These individual pulse properties, however, are of crucial importance for time-resolved studies or, in particular, for experiments elucidating nonlinear phenomena, for instance, two-photon double ionization (TPDI) of atoms [4,5] and molecules [6,7]. Here, the pulse-shape properties need to be known precisely when used as input parameters in modern *ab initio* theories to be benchmarked by the measurements (for a recent work, see, for example, Ref. [8]). Therefore, diagnostics of the pulse profile is crucial for monitoring and understanding the FEL source itself and, moreover, for a precise interpretation of the dynamics investigated.

Intensity autocorrelation is one of the most common methods to measure ultrashort pulse durations. It is based on nonlinear processes occurring either in crystals as commonly used or in atoms and molecules. Here, the absorption of  $n$  photons might lead to multiple ionization with the ion yields ( $Y^{(q+)}$ ) in a certain charge state  $q$  being proportional to the

intensity ( $I$ ) to the  $n$ th power  $Y^{(q+)} \propto I^n$  for nonlinear reaction pathways. Thus, measuring the respective ion yield for two pulses separated in time by a well-controlled and adjustable delay represents an  $n$ th-order autocorrelator. Consequently, the full width at half maximum (FWHM) of the pulse in the time domain can be extracted from an autocorrelation trace (i.e., a scan of the delay between the two pulses over their entire temporal envelope). Recently, the second-order autocorrelation measured at FLASH via so-called nonsequential TPDI of He [9,10] revealed pulse durations of about 30 fs assuming a Gaussian shape. Moreover, a value for the temporal coherence of 6 fs extracted previously in linear autocorrelation experiments assuming a temporal substructure of the SASE pulses with two leading 6-fs spikes separated by 12 fs and a fainter trailing pulse after 40 fs [11] was found to be consistent with the data, even though the statistical significance was not sufficient for an unambiguous proof. Qualitatively, such a structure was confirmed later by terahertz-streaking measurements [12] finding single spikes as short as 7 fs. More recently, linear autocorrelation measurements at different wavelengths [13] were in accord with the earlier ones [11], however, a monotonic behavior of the autocorrelation function was found without any substructure visible.

In this Rapid Communication, we report on a fourth-order autocorrelation trace measurement, expected to be very sensitive to the spatial and temporal coherence properties of the FEL pulses due to the high degree of nonlinearity, realized by selecting a certain dissociation channel (N<sup>2+</sup> + N<sup>2+</sup>) for N<sub>2</sub> molecules induced by the absorption of four 45.5-eV photons. The partial-coherence method developed recently [14] was employed to examine the influence of partial coherence on the observed data in a molecular dynamics measurement.

Our experimental setup at FLASH comprises a reaction microscope (REMI) [15] equipped with an on-axis back-reflection split-mirror setup for focusing and pulse-pair creation as schematically depicted in Fig. 1. It consists of a spherical multilayer mirror (1-in. Mo/Si mirror, 50-cm focal length) that is cut into two identical half mirror. While one half mirror is mounted at a fixed position, the other one is movable along the FEL beam axis by means of a high-precision piezostage, which

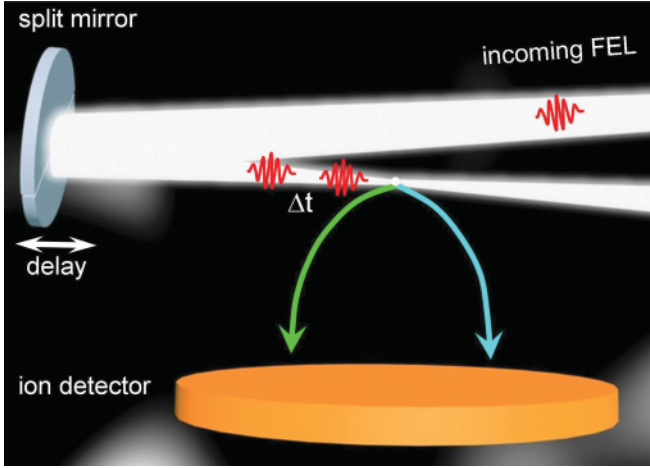


FIG. 1. (Color online) Schematic of the experimental setup with split-mirror stage and ion-detection part of the reaction microscope.

leads to an adjustable time delay up to  $\pm 2$  ps at a resolution of better than 1 fs. The mirror has a reflectivity of  $\approx 30\%$ , peaked around 45.5 eV with an FWHM of 3 eV such that higher-order harmonic radiation from the FEL is efficiently suppressed. During measurements, the intensity of the incoming FEL beam (10-mm diameter) was equally distributed over both half mirrors, and the foci were merged inside a dilute and well-localized beam (less than 1-mm diameter) of cold  $N_2$  molecules in the center of the REMI. With a focus diameter of  $\sim 20$   $\mu\text{m}$  and pulse energies of a few microjoules at an estimated average pulse duration of  $\sim 40$  fs, we reached peak intensities of  $I \cong 1 \times 10^{13}$  W/cm<sup>2</sup>. The overlap of the two focal points was initially adjusted observing the optical interference pattern obtained with a fiber-coupled diode laser with reduced coherence length aligned along the beam line with  $\sim 100$ - $\mu\text{m}$  precision. Further adjustment and fine-tuning were performed using a spatial imaging system for the created ions and the nonlinear  $N^{2+}$  signal. Ionic fragments were projected by means of an electric field (40 V/cm) onto a time- and position-sensitive detector (diameter 120 mm, position resolution 0.1 mm) and recorded as a function of the time delay. From the measured time of flight and position of each individual fragment, the initial three-dimensional momentum vectors were reconstructed.

The partial-coherence model (PCM) applied here, for the interpretation of the experimental data, is described in Ref. [14]. Briefly, the FEL spectral electric field is described as  $E_0(\omega) = \tilde{A}_0(\omega) \exp[i\tilde{\varphi}_0(\omega)]$  with the spectral amplitude  $\tilde{A}_0(\omega) = \sqrt{\tilde{I}(\omega)}$  given by a Gaussian fit to the measured average frequency spectrum  $\tilde{I}(\omega)$  (see Fig. 4). Using initially random spectral phases  $\tilde{\varphi}_0(\omega)$ , the temporal electric field  $E_0(t)$  is calculated by Fourier transformation, yielding a field that is infinitely long. To match the experimental FEL-pulse duration, the final electric field  $E(t) = E_0(t)F_0(t)$  is constructed by multiplying this initial field  $E_0(t)$  with a Gaussian (or any other) temporal filter function  $F_0(t)$  with its width corresponding to the measured average pulse duration of the FEL pulse. Due to the pulse-by-pulse random choice of  $\tilde{\varphi}_0(\omega)$ , the obtained temporal fields  $E(t) = F_0(t)E_0(t)$  after temporal filtering will be different for each FEL pulse. The

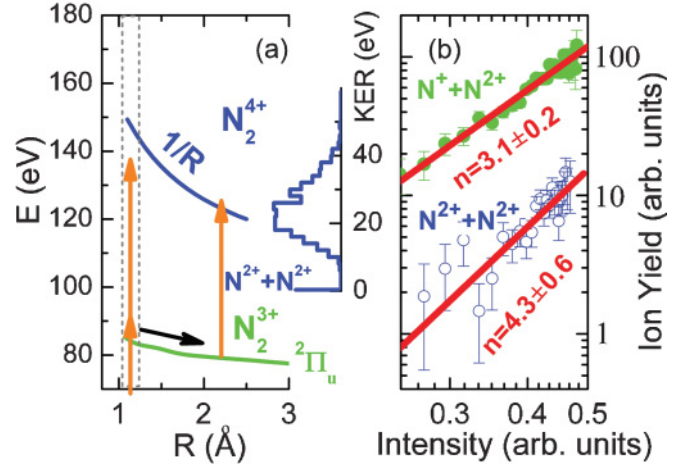


FIG. 2. (Color online) (a) Potential curves of  $N_2^{3+}(^2\Pi_u)$  [16] and  $N_2^{4+}$  (pure  $4/R$  Coulomb potential) together with the experimental KER distribution for  $N^{2+} + N^{2+}$  production for pump-probe delay times  $\tau < \pm 15$  fs. The vertical arrows indicate possible transitions at different  $R$ . Vertical dashed lines mark the Franck-Condon regime. (b) Intensity dependence of ion yields for the  $N^{2+} + N^{+}$  and  $N^{2+} + N^{2+}$  dissociation channels. The number  $n$  of absorbed photons is extracted from exponential fits (lines).

quality of the reconstructed pulse shapes can be confirmed, for example, by comparing the simulated average frequency spectrum  $\tilde{I}(\omega)$  with the measured one (Fig. 4).

By virtue of its construction, the PCM reproduces the shot-by-shot temporal (or spectral) electric fields (see Ref. [14]) in qualitative agreement with measured ones [11] and, moreover, allows one to construct the  $n$ th-order nonlinear autocorrelation trace, which is important in the present context ( $\tau$  is the pulse-to-pulse delay time):

$$S(\tau) = \int_{-\infty}^{+\infty} |[E(t) + E(t + \tau)]|^n dt. \quad (1)$$

As mentioned before, the number  $n$  of absorbed photons can be extracted from the measured intensity-dependent ion yields. In Figs. 2(a) and 2(b), schematic potential curves for  $N_2^{3+} \rightarrow N^{+} + N^{2+}$  and  $N_2^{4+} \rightarrow N^{2+} + N^{2+}$  Coulomb explosion channels are shown along with their measured respective population (ion) yields as a function of the intensity  $I$  indicating that three or four photons are needed to create triply or quadruple-charged ions, respectively.

Inspecting the potential curves in Fig. 2(a), this seems surprising for the  $N_2^{3+}$  channel because the  $N_2^{3+}(^2\Pi_u)$  state can already be reached by the absorption of two photons. However, since the many-particle (three electrons and one ion) final-state phase space becomes infinitely small at threshold, three-photon absorption dominates  $N_2^{3+}$  production at the present photon energies and intensities, a behavior that has been observed before under similar conditions [17]. Likewise, the so-called nonsequential (or direct) absorption of four photons would allow one to reach the  $N_2^{4+}$  final state through virtual intermediate levels in the Franck-Condon region of the neutral  $N_2$  molecule producing high-energetic fragments with a sum energy of about 40–50 eV. Those are, however, not observed in the kinetic-energy release (KER) spectra of coincident  $N^{2+} + N^{2+}$  ions for overlapping pump-probe pulses

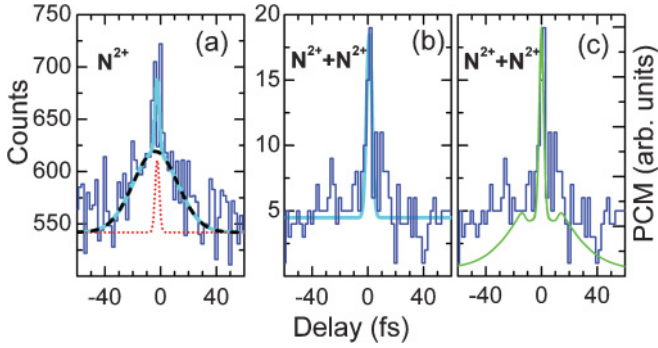


FIG. 3. (Color online) (a) Experimental autocorrelation traces for uncorrelated  $N^{2+}$  fragments with  $22 < E_{\text{KER}} < 40$  eV and restricted emission angles of  $45^\circ < \theta < 135^\circ$  with respect to the laser polarization axis. Solid cyan line: sum of two Gaussians with FWHM of 40 and 4 fs, respectively. (b) Same as in (a) but for coincident  $N^{2+} + N^{2+}$  data integrated over all emission angles. Solid cyan line: Gaussian fit with 4-fs FWHM. (c) Same experimental data as in (b) but compared with PCM result (full green line) normalized to the same maximum value as the experiment.

[i.e., at delay times  $\tau = 0 \pm 15$  fs as shown in Fig. 2(a)]. Rather, we find significantly smaller values of  $E_{\text{KER}} \approx 30$  eV indicating that the  $N_2^{4+}$  molecular ions are predominantly populated sequentially (i.e., from the dissociating  $N_2^{3+}$  state by absorption of one additional photon after some time): With the absorption of three photons, a dissociative wave packet is launched on the  $N_2^{3+}(^2\Pi_u)$  potential curve at an internuclear distance of  $R \approx 1.1$  Å that reaches  $R \approx 2.0$  Å after about 12 fs as estimated within classical propagation calculations. Here, the  $N_2^{4+}$  potential curve can be reached by the absorption of one additional photon, which now proceeds with a large cross section as it resembles an independent sequential-in-time single-ionization process of a triply charged molecule in the  $N_2^{3+}(^2\Pi_u)$  state neither requiring virtual intermediate states nor facing the many-particle phase-space limitations mentioned before. Clearly,  $N^{2+} + N^{2+}$  fragments with  $E_{\text{KER}} \approx 30$  eV can be seen in Fig. 3 for  $\tau = 0 \pm 15$  fs, well within the 12 fs needed to reach  $R \approx 2.0$  Å.

By integrating events in the region of  $E_{\text{KER}} = 30 \pm 8$  eV, we obtain the autocorrelation traces shown in Fig. 3. Both noncoincident  $N^{2+}$  and coincident  $N^{2+} + N^{2+}$  fragmentation channels are displayed in Figs. 3(a)–3(c), respectively. In order to avoid possible contributions from  $N^{2+} + N^{3+}$  breakup for the noncoincident  $N^{2+}$  ions in Fig. 3(a), we have only recorded ions emitted into an angular window of  $45^\circ < \theta < 135^\circ$  with respect to the polarization direction. Inspecting the azimuthal angular emission pattern for the  $N^{2+} + N^{3+}$  channel shows predominant emission parallel to the light polarization  $\vec{e}$ , in contrast to the  $N^{2+} + N^{2+}$  channel, which is mainly fragmenting perpendicular to  $\vec{e}$ . Note, contributions from breakup into  $N^+ + N^{2+}$  leads to lower KER and, thus, are rejected as well.

Surprisingly, at first glance, knowing that the average FEL-pulse duration is on the order of tens of femtoseconds, an extremely sharp peak is apparent at zero-delay time in both spectra, which can be well described by a Gaussian fit with an FWHM of  $4 \pm 1$  fs. The noncoincidently measured  $N_2^{2+}$  events [Fig. 3(a)] display a second component with a time

duration of  $40 \pm 10$  fs in agreement with expectations based on the temporal envelope of the FLASH pulses (for this fit, the FWHM for the sharp peak was fixed to 4 fs extracted from the autocorrelation trace for coincident  $N^{2+} + N^{2+}$ ).

In order to analyze these findings, we compare the experimental data with the PCM simulation in Fig. 3(c). Here, along the previous discussion, we have assumed the absorption of four photons in total and have included the molecular dynamics on the  $N_2^{3+}(^2\Pi_u)$  potential surface where the wave packet needs  $\sim 12$  fs to reach an internuclear distance where the  $N_2^{4+}$  potential curve can be reached by the sequential absorption of one additional photon. We calculate the yield of  $N^{2+} + N^{2+}$  fragments as a function of the pulse delay time  $\tau$  by

$$S(\tau) = \int_{t=-\infty}^{\infty} \int_{t'=-\infty}^t [|E(t') + E(t' + \tau)|^2]^3 |E(t + t_{\text{mol}}) + E(t + t_{\text{mol}} + \tau)|^2 dt' dt, \quad (2)$$

where the first term reflects the creation of dissociating  $N_2^{3+}$  molecular ions by nonlinear three-photon absorption from the neutral ground state and the second part accounts for the subsequent one-photon transition from the triply charged to the final  $N_2^{4+}$  state. The delayed onset of the second ionization step for  $R > 2.0$  Å is taken into account by introducing an intrinsic time delay of  $t_{\text{mol}} = 12$  fs. Note that our simulations include the spatial averaging in the noncollinear pump-probe geometry by averaging over a few optical periods along the  $\tau$  coordinate, otherwise the PCM result shows fast optical-cycle time-scale modulations. In agreement with the measurement, the simulation averaged over 3160 simulated pulses displays two components in the autocorrelation trace (i.e., one sharp peak on the top of a broad one). Whereas the broad component is always present in the simulations, essentially resembling the FWHM of the FEL-pulse time envelope, the relative intensity between the sharp and the broad contribution is governed by the spatial coherence properties of the FEL pulses. In the simulation, it is assumed that the foci of the two pulses from the split-mirror setup are perfectly overlapping in space and that both beams are fully spatially coherent. Under these conditions, that are certainly only partly fulfilled in the experiment, we obtain a relatively high contribution of the sharp peak, indicating that the transverse coherence length in the present measurement is on the order of a few millimeters or longer (for recent spatial coherence measurements at FLASH, see Refs. [11,18]). Different from the second-order autocorrelation trace simulated in Ref. [14], the broader component is partially structured with a minimum between the sharp and the broad components, which is due to the  $\sim 12$ -fs time threshold imposed by the molecular dynamics of the sequential second ionization step. Within present statistics, this dip is not discernible in the experimental data.

On the basis of the analysis within the PCM, we, thus, interpret the  $\sim (40 \pm 10)$ -fs component in the autocorrelation trace to closely resemble the average pulse duration in the present experiment, whereas the sharp spike of  $4 \pm 1$  fs can largely be related to the longitudinal coherence of the FLASH pulse. Both observations are consistent with the results of earlier temporal pulse profile measurements at 23.9 nm [9,11] (streaking at 13.5 nm [12]) where pulse durations of  $29 \pm 5$  fs ( $35 \pm 7$  fs) and coherence times of 6 fs [11] were extracted



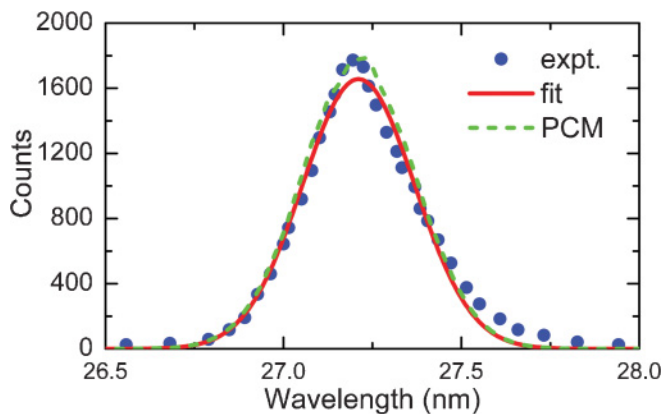


FIG. 4. (Color online) Measured average frequency spectrum. Solid line: Gaussian fit. Dashed line: result of PCM.

(limited by the experimental resolution). Different from the earlier experiments [9,11], however, we do not need to assume a certain typical time in between the spikes within one pulse.

Knowing that the final step can only take place after a finite time  $t_{\text{mol}}$ , dictated by the molecular dynamics in the fragment KER regime observed, one might be surprised though, that the sharp spike occurs at a delay time equal to zero and not after 12 fs. This is because the autocorrelation trace is dominated by the first nonlinear three-photon absorption step to the  $\text{N}_2^{3+}$  potential, which is most efficient for zero time delay between the two pulses, combined with the feature that the pulse envelope is long enough such that the second step, the additional absorption of a single photon populating the  $\text{N}_2^{4+}$  final state, can still take place in the trailing part of the pulse at zero delay. Therefore, in the present case and for the KER regime investigated, the molecular dynamics only manifests itself in the much weaker peak occurring for a delay of 12 fs in the simulation, which would only dominate for pulse envelopes shorter than  $t_{\text{mol}}$ . This is not true if the first potential surface can be reached with a single photon already making both steps similarly efficient and leading to respective peaks in pump-probe experiments at delay times directly resembling the molecular dynamics as demonstrated recently for wave packets on the  $\text{D}_2^+$  potential surface [19].

Further information on the longitudinal coherence length can be extracted from the spectral distribution measured in

parallel (Fig. 4) along with the PCM simulation, in excellent agreement with the experimental data. Fitting the spectrum with a Gaussian function results in an FWHM of 0.37 nm corresponding to an estimated minimum coherence time of 3 fs on the basis of the Heisenberg uncertainty principle, which is very close to our observation of about 4 fs as well as to the expected cooperation length within the electron bunch [11].

To summarize, by selecting a highly nonlinear multiple ionization reaction, producing  $\text{N}_2^{4+}$  molecular ions by the absorption of four photons, as a fourth-order autocorrelator, we find signatures of the temporal coherence length of FLASH pulses in the nonlinear autocorrelation trace, which reveals a pulse duration of  $40 \pm 10$  fs with a coherence time of about  $4 \pm 1$  fs related to the internal SASE-pulse time structure. A partial-coherence approach was employed to simulate the experimental observations, and excellent agreement with the experimental results is found taking the molecular dynamics that is involved into account.

Our results have important consequences for the achievable time resolution in split-beam pump-probe experiments using spiky SASE FEL pulses that have already become apparent in a previous measurement by us [19] exploring the wave-packet dynamics of  $\text{D}_2^+$  molecular ions. In light of the present results, we now see that time resolutions close to the temporal coherence time of the FEL radiation can be achieved with pulse-envelope durations that are substantially longer. This opens, for example, the exciting possibility to perform x-ray-x-ray pump-probe experiments with attosecond time resolution at X FELs. On the basis of recent FEL simulation calculations at a wavelength of 1.5 Å and a pulse envelope of about 2 fs [3], time resolutions as good as  $\sim 300$  as can be expected in future split-mirror arrangements that are presently being designed.

The authors are greatly indebted to the scientific and technical team at FLASH, in particular, the machine operators and run coordinators, in striving for optimal beam-time conditions. Support from the Max-Planck Advanced Study Group at CFEL is gratefully acknowledged. Y.H.J. acknowledges support from DFG Project No. JI 110/2, T.P. from the MPG-MPRG program, X.L. and K.U. from MEXT via the XFEL Utilization Research Project, O.H., M.L., and M.F.K. from the DFG via the Emmy-Noether program and the Cluster of Excellence: Munich Center for Advanced Photonics.

- 
- [1] T. Shintake *et al.*, *Nature Photon.* **2**, 555 (2008).
  - [2] W. Ackermann *et al.*, *Nature Photon.* **1**, 336 (2007).
  - [3] Y. Ding *et al.*, *Phys. Rev. Lett.* **102**, 254801 (2009).
  - [4] A. A. Sorokin *et al.*, *Phys. Rev. A* **75**, 051402(R) (2007).
  - [5] A. Rudenko *et al.*, *Phys. Rev. Lett.* **101**, 073003 (2008).
  - [6] H. Fukuzawa *et al.*, *J. Phys. B* **42**, 181001 (2009).
  - [7] Y. H. Jiang *et al.*, *Phys. Rev. A* **81**, 021401(R) (2010).
  - [8] M. Kurka *et al.*, *New J. Phys.* **12**, 073035 (2010).
  - [9] R. Mitzner *et al.*, *Phys. Rev. A* **80**, 025402 (2009).
  - [10] F. Sorgenfrei *et al.*, *Rev. Sci. Instrum.* **81**, 043107 (2010).
  - [11] R. Mitzner *et al.*, *Opt. Express* **16**, 19909 (2008).
  - [12] U. Fröhling *et al.*, *Nature Photon.* **3**, 523 (2009).
  - [13] W. F. Schlotter *et al.*, *Opt. Lett.* **35**, 372 (2010).
  - [14] T. Pfeifer *et al.*, *Opt. Lett.* **35**, 3441 (2010).
  - [15] J. Ullrich *et al.*, *Rep. Prog. Phys.* **66**, 1463 (2003).
  - [16] A. D. Bandrauk *et al.*, *Phys. Rev. A* **59**, 4309 (1999).
  - [17] Y. H. Jiang *et al.*, *Phys. Rev. Lett.* **102**, 123002 (2009).
  - [18] A. Singer *et al.*, *Phys. Rev. Lett.* **101**, 254801 (2008).
  - [19] Y. H. Jiang *et al.*, *Phys. Rev. A* **81**, 051402(R) (2010).